Experimental and theoretical electronic structure determination for PtSi

N. Franco,[1] J. E. Klepeis,[1] C. Bostedt,[1] T. Van Buuren,[1] C. Heske,[2] O. Pankratov,[3] T. A. Callcott,[4] D. L. Ederer,[5] and L. J. Terminello[1]

[1]*Lawrence Livermore National Laboratory, University of California, Livermore, California 94551, USA*
[2]*Universität Würzburg, D-97074 Würzburg, Germany*
[3]*Universität Erlangen-Nürnberg, D-91058 Erlangen, Germany*
[4]*Physics Department, University of Tennessee, Knoxville, Tennessee, 37996, USA*
[5]*Department of Physics, Tulane University, New Orleans, Louisiana, 70118, USA*

We present a complete experimental and theoretical electronic structure study of PtSi using a combination of synchrotron radiation photoelectron spectroscopy (SR-PES), soft x-ray emission spectroscopy (SXE), x-ray absorption spectroscopy (XAS), and first principles electronic structure calculations. We have carried out both SXE and XAS measurements of the Si $L_{2,3}$ edge, which probe the Si $3s$ and $3d$ partial density-of-states (PDOS) in the valence and conduction bands, respectively. We have also obtained SR-PES data at photon energies of 80 and 130 eV for the valence band of PtSi. By taking advantage of the Cooper minimum effect we are able to probe the contribution of the Pt $5d$ orbitals. As an aid to interpreting the experimental spectra we have performed first principles calculations of the PDOS for the Pt $6p$ and $5d$ as well as the Si $3s$, $3p$, and $3d$ orbitals. We have carried out core-level PES measurements for Pt $4f$ and Si $2p$ and find a double shift in which both core levels are shifted to higher binding energy. First principles calculations confirm the presence of this double shift. Our combined experimental and theoretical results lead us to conclude that the Pt $5d$ orbitals are not highly localized as has been assumed in all previous experimental studies of PtSi. Rather we find that the influence of the $5d$ orbitals extends throughout the whole valence band and that the nature of the chemical bonds is more complex than the earlier studies have assumed. Our first principles calculations of the energy-resolved electronic charge density confirm this interpretation.

I. INTRODUCTION

In recent years the technological importance of metal silicides has motivated an increasing interest in both their fundamental and applied characteristics. Some of these silicides play a crucial role in silicon-based semiconductor technology since they are widely used in ohmic and rectifying (Schottky) contacts.[1–3] The high conductivity,[4] thermal stability,[5,6] and silicon compatibility[4,6] of transition-metal silicides make them good candidates for infrared sensors,[7–12] ultraviolet or vacuum ultraviolet photodetectors,[13,14] and polysilicon interconnects.[4,6,8,11,15–17] Noble-metal silicides have been the focus of attention because they do not form insulating metal oxides during processing as electrode materials for semiconductor memory devices.[18] This collection of properties has encouraged an extensive number of silicide-related studies.[6,19]

Ti$_2$Si is probably the most used and best understood silicide due to the success of its application in polysilicon interconnects.[4,6] However, the sheet resistance of Ti$_2$Si increases dramatically when one of the dimensions is reduced.[20] In sub-half-micron technologies PtSi and NiSi have been shown to be good candidates for replacing Ti$_2$Si since their structural and electronic properties are less sensitive to lateral or vertical size.[21,22] Nonetheless, PtSi is probably one of the least understood silicides in contrast to the extensive knowledge that exists for Ti$_2$Si. For example, most of the experimental studies to date have simply assumed that the electronic structure of PtSi is similar to that of other transition-metal silicides. We are aware of no prior study in

which theory and experiment have been combined to provide a complete and accurate electronic structure characterization of PtSi.

However, many different techniques have been used to characterize the growth properties of PtSi, including the phase growth sequence,[23–30] growth kinetics,[24,28–34] growth rates,[30,34] role of impurities,[18,35–39] stoichiometry,[24,30,40] stability of solid-state reaction products,[5,16,41] mass transport across the reaction interface,[33] and microstructure or epitaxial film formation.[11,40,42–48] Since the initial steps in a thin film deposition process generally influence the final product, most of the previously published studies have focused not only on bulk PtSi, but also on the initial Pt/Si interface. A summary of the experimental techniques used in all of these studies includes transmission electron microscopy,[27] x-ray photoelectron spectroscopy (XPS),[26,49–55] Auger electron spectroscopy (AES),[27,53,55,56] ultra-violet photoelectron spectroscopy (UPS),[27,49,52,53,57–60] low energy electron diffraction,[56] soft x-ray emission spectroscopy (SXE),[61] x-ray absorption spectroscopy (XAS),[62,63] surface extended x-ray absorption fine structure,[53] grazing incidence diffraction,[48] and Raman spectroscopy.[53]

Recently Stark *et al.*[30] used ellipsometry measurements to study the kinetic parameters for PtSi formation. Wang *et al.*[26] have also characterized the kinetic growth sequence and they obtained results that differ from those of Stark *et al.*[30] As a complement to these more applied studies, and in order to better understand the physics of silicide formation, it is desirable to perform studies at a more fundamental level. A complete characterization of the atomic and electronic struc-

ture of PtSi should help to resolve the ambiguities in the previously reported studies, and also establish the underlying basis for the technological applications of this material.

In contrast to the experimental studies, the number of previous theoretical studies is very small. Beckstein *et al.*[64] recently carried out first principles electronic structure calculations for Pt_2Si and PtSi. In addition to the electronic structure, they also calculated all of the equilibrium structural parameters and zero-pressure elastic constants for both phases. Klepeis *et al.*[65] studied the fundamental nature of the chemical bonding and elasticity in these same two silicides by constructing valence force field models fit to the elastic constants calculated by Beckstein *et al.*[64] There have also been calculations of the angular-momentum-resolved density of states (DOS),[53,58,66] and a comparison between XPS and SXE measurements and the calculated electronic structure for different $4d$ and $5d$ transition-metal silicides.[67]

Despite the large number of experimental studies, many of the more fundamental properties of PtSi have not been fully addressed experimentally. Examples include the nature of the chemical bonding, the contribution of different orbitals to the valence band (VB), and the charge transfer between the atoms. In addition, there remain a number of controversies such as the disagreement between theory and experiment with regard to the electronic structure at the Fermi energy (E_F),[67] the nature of the charge transfer between Pt and Si,[53] and a satisfactory explanation of the VB electronic structure.[67]

In this paper we present a complete theoretical and experimental electronic structure study of PtSi by means of synchrotron radiation photoelectron spectroscopy (SR-PES), SXE, and XAS. By using the SR-PES technique we can measure the total DOS (TDOS) for the VB or extract information about the chemical bonding by means of core-level photoelectron spectroscopy (CL-PES). In addition, SXE and XAS are excellent tools for determining the orbital-specific partial DOS (PDOS) for the VB (filled states) and the conduction band (CB) (empty states), respectively, by taking advantage of the dipole selection rules for electronic transitions. PES is a surface sensitive technique while SXE and XAS probe the bulk [if the partial fluorescence yield (PFY) mode is used]. Our *ex situ* prepared samples suffered from surface contamination but since SXE and XAS both probe the bulk we were nonetheless able to make measurements and direct comparisons between *in situ* and *ex situ* prepared samples. In order to present a more complete picture, first principles electronic structure calculations for PtSi were also carried out and compared with our experimental results and previously published data. A preliminary account of the work described here has appeared previously.[68]

The remainder of this paper is organized as follows. Section II contains a description of the experimental and theoretical techniques. Section III briefly summarizes the kinetic growth model for PtSi prepared on a Si substrate. Section IV presents and compares the experimental measurements and theoretical calculations and is divided into three parts. Section IV A focuses on the PtSi VB and CB electronic structure, Sec. IV B discusses the Pt $4f$ and Si $2p$ CL-PES data and deduces the chemical bonding properties of the silicide,

and Sec. IV C describes calculations of the energy-resolved electronic charge density in order to further clarify our interpretation of the experimental spectra. A summary and conclusions are given in Sec. V.

II. EXPERIMENTAL AND THEORETICAL TECHNIQUES

Both the atomic and electronic structures of a material are generally needed in order to provide a basic understanding of the properties of that material, including the optical, electrical, magnetic, and mechanical properties. However, atomic and electronic structures are strongly correlated and full knowledge of one typically enables an understanding of key parts of the other. Experimental and theoretical methods now exist that can be used to accurately obtain the electronic structure of most materials. With the advent of synchrotron radiation facilities, spectroscopic methods (XPS, UPS, XAS, SXE, etc.) have been successfully developed such that they represent one of the best choices for electronic structure characterization. On the theoretical side, first principles methods have been shown to provide accurate electronic and atomic structure information for a wide range of materials systems.

A. Experiment

In solid-state physics most materials can be described using classical band theory where the VB and CB are responsible for the chemistry-related properties of the solid. These bands can be probed using different spectroscopic techniques; XAS,[69] SXE,[70] and PES (Ref. 71) are currently among the more popular choices. In XAS an electron is excited from a core level into an unoccupied state of the CB (just above E_F) and changes in the sample current [total electron yield (TEY)] or the fluorescence emission (PFY) are measured while scanning across the relevant threshold (K, L_1, or $L_{2,3}$ in our case). The measured intensity as a function of energy is a PDOS projected onto the core hole potential appropriate to the final state.[72] Changes in the spectrum can also be observed due to changes in the potential of the initial state.[72]

SXE is used to map out the VB PDOS allowed by the dipole selection rules. In this case fluorescence spectra are produced when x rays are used to excite characteristic emission lines. In recent years powerful third generation synchrotron sources have made possible the measurement of very low fluorescence yields for radiative transitions in the soft x-ray regime. The particular advantage of SXE over PES in probing the VB is the possibility of selecting specific orbitals and thus obtaining the PDOS.

In the case of PES, photoemitted electrons are collected from a core level or VB state after exciting the atom with energetic photons. This method can be used to probe either changes in the electronic structure and bond character at the core level (with respect to a reference sample) or the total density of states (TDOS) of the VB.[73] There are two energy-dependent factors that dominate the photoemission process.[74] The photoionization cross section σ determines the probability of excitation for a specific electronic level while the elec-

tron escape depth (EED) is the mean free path that the excited electron travels across the sample on its way out to the vacuum. The tunability of the photon energy $h\nu$ when using synchrotron radiation sources creates the possibility for taking advantage of the energy dependence of these two factors in order to study different electronic characteristics of a material. A notable consequence of this dependence on $h\nu$ is the Cooper minimum effect.[75] In some atoms the radial part of the initial state wave function can have strong variations such that there is a significant reduction in the transition matrix element at particular energies. This reduction translates into a minimum in σ that is called a Cooper minimum. The net result is that σ can vary by orders of magnitude for different one-electron orbitals by varying $h\nu$. Therefore, by tuning $h\nu$ appropriately, we can differentiate between different orbital contributions and thus measure not only the TDOS but also the PDOS.

In our experiments we used two sets of samples, one prepared *in situ* under ultra high vacuum (UHV) and another provided by ZAE-BAYERN (Erlangen, Germany). In the former case, an n-type (phosphorous-doped, $\rho = 11$–$25 \ \Omega$ cm) Si(100) single-crystal substrate was thermally cleaned and checked by SR-PES, paying particular attention to the amount of carbon, oxygen, and nitrogen. No traces of these contaminants were found prior to the evaporation of Pt in any of the *in situ* prepared samples. The silicide preparation and data acquisition were both carried out under UHV, with a base pressure of 4×10^{-11} Torr. We resistively evaporated Pt from an ultrapure filament, checking the coverage and cleanliness of the as-deposited Pt by measuring the ratio between the Si $2p$ and Pt $4f$ core levels. Accounting for variations in the EED of the measured electrons and in σ at selected values of $h\nu$ (130, 208, 400, and 800 eV), we found that the Pt coverage was always larger than 20 Å (after the Pt evaporation no traces of the Si $2p$ core level peak were found). Thin films of Pt_2Si and PtSi were prepared by resistively annealing the substrate at different temperatures. These temperatures were calibrated with an optical pyrometer. During the annealing process the pressure of the system was always better than 4×10^{-10} Torr. The cleanliness of the annealed silicide film was always checked using SR-PES and no traces of any contaminant species were found.

We also used samples of PtSi grown *ex situ* and provided by ZAE-BAYERN to determined the PDOS at the VB and CB by means of SXE and XAS. These samples were prepared using a p-type Si(100) single crystal ($\rho = 17$–$25 \ \Omega$ cm). A Pt coverage of 35 nm was evaporated *in situ* (evaporation rate of 0.02 nm/s) and annealed *in situ* at 300 °C until a thin film of PtSi was formed.

In acquiring the experimental data we have taken advantage of the high flux, high resolution, and small spot size of the IBM/TENN/TULANE/LLNL/LBL undulator beamline 8.0.1 at the Advanced Light Source synchrotron radiation facility in Berkeley, California. VB and core level SR-PES spectra were obtained using the ellipsoidal mirror analyzer at the 8.0.4 end-station. The SXE and XAS data of the VB and CB were obtained using the Rowland circle x-ray emission

spectrometer located at the 8.0.1 end-station. Detailed descriptions of these two spectrometers have been given elsewhere.[76,77]

B. Theory

The calculated PDOS and electronic charge densities were obtained using a full-potential linear muffin-tin orbital (FP-LMTO) method[78,79] that makes no shape approximation for the crystal potential. The crystal is divided up into regions inside atomic spheres, where Schrödinger's equation is solved numerically, and an interstitial region. As in all LMTO methods the wave functions in the interstitial region are Hankel functions. An interpolation procedure is used for evaluating interstitial integrals involving products of Hankel functions. The triple-κ basis is composed of three sets of s, p, d, and f LMTOs per atom with Hankel function kinetic energies of $-\kappa^2 = -0.3$, -1.0, and -2.3 Ry (48 orbitals per atom). The Hankel functions decay exponentially as $e^{-\kappa \cdot r}$. The angular momentum sums involved in the interpolation procedure are carried up to a maximum of $\ell = 6$. The calculations presented here are based on the local density approximation (LDA), using the exchange-correlation potential of Ceperley and Alder[80] as parametrized by Vosko, Wilk, and Nusair.[81] The scalar-relativistic Schrödinger equation was solved self-consistently for orthorhombic PtSi. We did not include spin-orbit interactions and we used atomic sphere radii equal to one-half the nearest-neighbor Pt–Si bond length. The effect of spin-orbit interactions would normally be large for Pt but in the case of PtSi the Fermi energy occurs well above the narrow d-derived bands, which are therefore completely occupied, thus reducing the impact of spin-orbit splittings.

The Pt $6s$, $6p$, $5d$, and $5f$ orbitals as well as the Si $3s$, $3p$, $3d$, and $4f$ orbitals were all treated as valence states. The semicore Pt $5s$ and $5p$ orbitals were treated as full band states by carrying out a "two-panel" calculation. The second panel band calculation for the semi-core orbitals included the Pt $5s$, $5p$, $5d$, and $5f$ orbitals as well as all of the Si valence orbitals. The Brillouin zone (BZ) sums were carried out using the tetrahedron method.[82] In the case of both the self-consistent total energy and charge density calculations we used a shifted $12 \times 16 \times 12$ ($6 \times 8 \times 6$) mesh in the full BZ, resulting in 288 (36) irreducible **k** points in the first (second) panel. For the purpose of calculating the PDOS we used an unshifted $16 \times 24 \times 16$ mesh that included the Γ point, corresponding to 1053 irreducible **k** points.

The atomic structure of orthorhombic PtSi corresponds to space group $Pnma$ (No. 62) with four symmetry-equivalent Pt atoms occupying $4(c)$ sites and four symmetry-equivalent Si atoms also occupying $4(c)$ sites. The unit cell is specified by three lattice constants a, b, and c. The positions of the atoms are not fully constrained by the space group alone but rather there are four internal structural parameters needed to determine the x and z coordinates of the Pt and Si atoms, x_{Pt}, z_{Pt}, x_{Si}, and z_{Si}. We have used the experimental atomic structure determined by Graeber *et al.*,[83] $a = 5.577$ Å, $b = 3.587$ Å, $c = 5.916$ Å, $x_{Pt} = 0.9956$, $z_{Pt} = 0.1922$, $x_{Si} = 0.177$, and $z_{Si} = 0.583$. Beckstein *et al.*[64] recently deter-
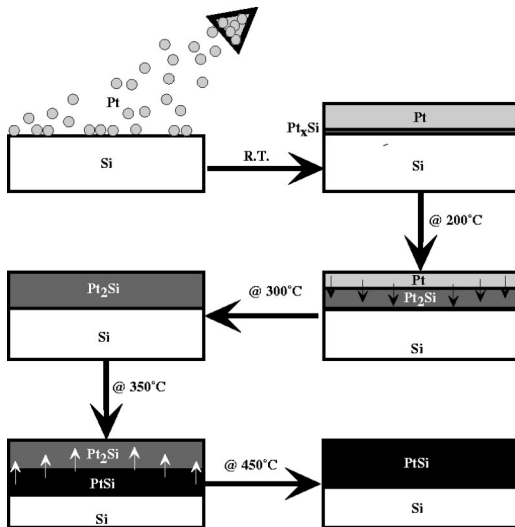
FIG. 1. Schematic diagram showing the different temperature-dependent steps during the formation of PtSi on a Si substrate. Depending on the cleanliness of the substrate and the thickness of the deposited Pt, some authors have suggested alternate temperature windows.

mined the theoretical minimum energy structure and find values of these parameters that are very close to the experimental numbers used here.

The angular-momentum-resolved PDOS were generated on the basis of a Mulliken decomposition,[84] as described by McMahan *et al.*[85] A Mulliken decomposition is inherently nonunique and this ambiguity is further compounded by the fact that we choose to project out against a particular set of orbitals, the numerical basis functions obtained from the self-consistent calculations. This projection clearly depends on the characteristics of these orbitals but the results are nonetheless useful because the most important characteristics of the orbitals are that they are localized and possess the appropriate symmetry properties.

III. KINETIC GROWTH MODEL

We briefly introduce the important elements of the generally accepted kinetic growth model for the preparation of PtSi on a Si substrate.[30] These elements are shown schematically in Fig. 1. A reaction occurs at the interface when Pt is deposited (by means of thermal evaporation, electronic evaporation, sputtering, etc.) on clean Si at room temperature. At submonolayer Pt coverages there are changes in the surface states that are big enough to allow the identification of variations in the atomic and electronic structure.[49,52,53] At Pt coverages of 2–5 ML the interface is silicidelike, while increasing the coverage (up to 20 ML) makes the interface become more "metal"-like. For sufficiently large coverages unreacted Pt remains on the surface. In the absence of thermal treatment a reaction takes place at the interface (only a few ML) in which Pt atoms migrate into the Si, forming a few silicidelike layers. This migration becomes negligible after a few ML, and there is a transition from silicidelike to pure Pt layers. Under annealing the situation is modified,

starting with the formation of the Pt_2Si phase at lower temperatures and followed by the formation of the PtSi phase at higher temperatures. The Pt_2Si phase is formed when the Pt atoms migrate into the Si, while the PtSi phase results from the migration of Si atoms back into the existing Pt_2Si layers.[30] There is general agreement regarding the annealing temperatures. Most studies have given a temperature range of 180–200 °C for the beginning of Pt_2Si formation,[15,30,37] while a temperature between 280 and 400 °C is generally reported as the lower limit for PtSi formation.[30,35]

Since a key factor in the formation of Pt_2Si and PtSi is the mobility of the Pt and Si atoms, respectively, another important element in the growth kinetics is the annealing time. Increasing the annealing time will give these atoms more opportunity to migrate and form the silicide. The appropriate annealing time is, of course, strongly correlated with the annealing temperature and the Pt coverage and therefore these three factors cannot be considered separately. However, it is generally accepted that all of the Pt is transformed into PtSi under the following conditions: low Pt coverages (under 100 Å), annealing temperatures as high as 600 °C, and annealing times of approximately 30 min. Finally, we note that the introduction of contaminant species can dramatically alter the kinetics of PtSi formation.[86] However, in our experiments we checked extensively for contaminants and therefore we conclude that we are working in a clean environment.

IV. RESULTS AND DISCUSSION

A. PtSi VB and CB electronic structure

In the independent-electron model the threshold transitions corresponding to the Si $L_{2,3}$ edge directly couple the initial state Si $2p$ core level with the Si $3s$ and $3d$ empty CB states. Thus, by monitoring the absorption coefficient modulation while scanning across the Si $L_{2,3}$ threshold (Si $2p \rightarrow$ Si $3s + 3d$ transition) we can investigate the Si $3s$ and $3d$ PDOS in the CB. In the transition-metal silicides the transition-metal d orbitals are more localized than the Si s orbitals and therefore transitions into the d states produce a so-called "white line" (d-like states have a jagged DOS and transition matrix elements that vary widely in comparison to s-like states). Conversely, transitions into s states yield absorption edges that are much smoother. In addition, by exciting an electron from the Si $2p$ core level into the CB and then observing the valence Si $3s + 3d \rightarrow$ Si $2p$ transitions, we can probe the Si $3s$ and $3d$ PDOS in the VB. In Fig. 2 we show Si $L_{2,3}$ SXE and XAS measurements together with the theoretical PDOS (Si $3s$ and $3d$ orbitals combined and the Si $3d$ orbitals only) for PtSi. The intensities of the SXE and XAS data were not measured on an absolute scale and so they are normalized with respect to the theoretical PDOS. The energy calibration was performed by shifting the spectra in accordance with a previously measured Si reference sample.[87]

In Fig. 3 we show the XPS spectra for PtSi obtained at $h\nu = 80$ and 130 eV. The TDOS obtained at $h\nu = 80$ eV primarily reflects the Pt $5d$ orbitals (σ for Pt $5d$ is almost an order of magnitude larger than for Pt $6p$, Si $3s$, and Si $3p$).
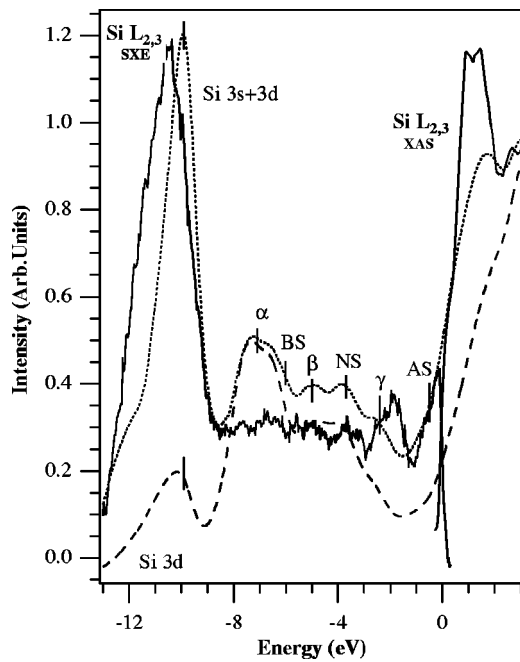
FIG. 2. Experimental and theoretical VB and CB PDOS for PtSi. The Si $L_{2,3}$ SXE and XAS spectra (solid lines) represent the experimental Si $3s$ and $3d$ PDOS. The calculated PDOS correspond to the TDOS projected onto the Si $3s$ and $3d$ orbitals (dotted line) and the Si $3d$ orbitals only (dashed line).

In the case of the TDOS obtained at $h\nu = 130$ eV, σ for Pt $5d$ is only 2.5 times larger than for Pt $6p$ and only five times larger than for Si $3s$ or Si $3p$.[53] We have also plotted the theoretical PDOS for all of the Pt orbitals combined (Pt $6s$,
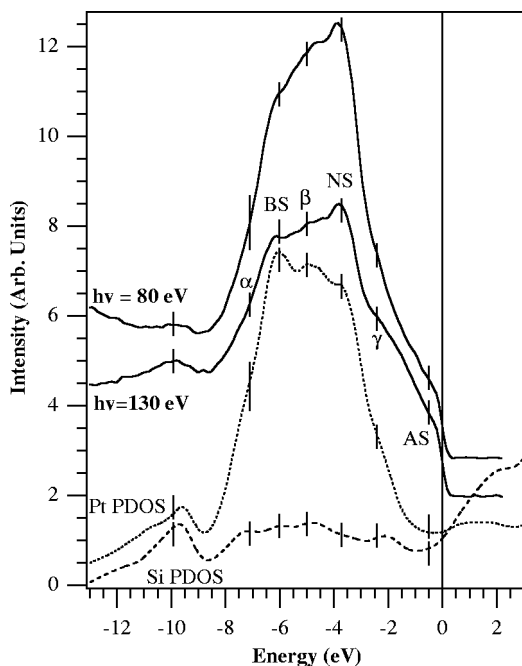

FIG. 3. Comparison between the VB XPS spectra (solid lines) obtained at $h\nu = 80$ and 130 eV. The calculated Pt PDOS (dotted line) and Si PDOS (dashed line) are also shown.
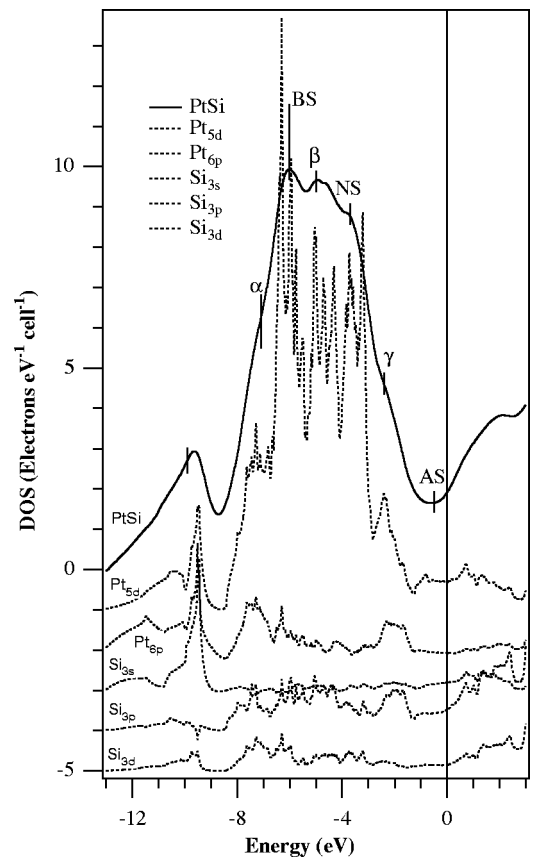

FIG. 4. Theoretical PtSi TDOS (solid line) and PDOS (dotted lines). The TDOS has been projected separately onto the Pt $6p$ and $5d$ orbitals as well as the Si $3s$, $3p$, and $3d$ orbitals. The TDOS is convoluted with a Lorentzian in order to account for the experimental resolution (0.6 eV), while the PDOS are unsmoothed.

$6p$, $5d$, and $5f$) and all of the Si orbitals combined (Si $3s$, $3p$, and $3d$).

In order to aid in the interpretation of the observed features in the experimental spectra we have also calculated the individual Pt and Si orbital contributions to the theoretical PtSi TDOS using a Mulliken decomposition. In Fig. 4 we show the unsmoothed theoretical PDOS for Pt $6p$ and $5d$ as well as Si $3s$, $3p$, and $3d$. Also shown is the PtSi TDOS convoluted with a Lorentzian in order to account for the experimental resolution (0.6 eV). On the basis of our experimental results we have divided the VB into four primary energy regions that we analyze below, in addition to the CB.

1. VB near −10.0 eV

The experimental Si PDOS in Fig. 2 exhibits a prominent peak near -10 eV (below E_F). This peak has been reported previously and is associated with the Si $3s$ orbitals. The conventional model for this peak is that it arises from the absence of Si sp^3 tetrahedral bonds in the silicide, which leaves the Si $3s$ orbitals unhybridized. This peak has been reported for nearly every silicide, and is therefore believed to be insensitive to the transition-metal–silicon bonding. Figure 2 shows the Si $L_{2,3}$ SXE spectrum that we have identified with the Si $3s$ and $3d$ PDOS. The experimental peak is

located at -10.3 eV while the theoretical one is at -9.9 eV. This small disagreement is not significant and can be explained by two factors. The first is the experimental resolution of approximately 0.6 eV, which results in a Si $L_{2,3}$ peak that is wider than the theoretical PDOS peak. A second explanation is the likely underestimate of the total bandwidth in the theoretical (LDA) PDOS. Since we have aligned the experimental and theoretical PDOS at E_F, the error due to the underestimated bandwidth will be largest at energies furthest from E_F. Finally, we note that the plot of the Si $3d$-only PDOS indicates that these orbitals contribute very little to the -10 eV peak.

Figure 3 provides additional information regarding the nature of the states near -10 eV. As a result of the Cooper minimum effect described in Sec. II A, the XPS measurements at $h\nu = 80$ eV should be similar to the Pt $5d$ PDOS, while at $h\nu = 130$ eV the spectra are expected to be a mixture of the Pt $5d$ and $6p$ PDOS plus smaller contributions from the Si $3s$ and $3p$ orbitals. Therefore, by comparing the XPS spectra at these two values of $h\nu$ we should be able to clarify the nature of the states. In the $h\nu = 80$ eV spectrum in Fig. 3 we see some intensity at -9.9 eV that becomes more prominent for $h\nu = 130$ eV. The fact that the intensity increases with increasing $h\nu$ confirms that this feature is not purely Pt $5d$ in character but rather that it has at least some contributions from Pt $6p$ or Si $3s$. In the same figure we also plot the theoretical Pt and Si PDOS for PtSi. The peak at -9.8 eV appears to have similar contributions from both the Pt and Si orbitals. The individual orbital contributions to this peak are shown in Fig. 4. We see that the Si $3s$ orbitals do indeed represent the dominant contribution but we also see that the Pt $5d$ and $6p$ orbitals play an important role. The presence of a contribution from the Pt $5d$ orbitals in the lower part of the VB is contrary to the prevailing model for chemical bonding in transition-metal silicides, which states that the d orbitals are very localized and not heavily involved in the bonding. Yarmoshenko *et al.*[67] have previously reported that the Si $3s$ orbitals are not mixed with the Pt $5d$ or $6p$ orbitals, while Yamauchi *et al.*[61] stated that the role of sd bonding was unclear. The idea that the Si $3s$ orbitals are not involved in the bonding is part of nearly every published study on transition-metal silicides. Nonetheless, on the basis of our combined theoretical and experimental results we conclude that at least some mixing between the Si $3s$ and Pt $5d$ or $6p$ orbitals occurs in the lower part of the VB in PtSi.

2. VB between -9.0 and -3.0 eV

In contrast to the situation for the peak near -10 eV where there was excellent agreement between theory and experiment, in the case of the region between -9.0 and -3.0 eV we see a number of small discrepancies. The $L_{2,3}$ SXE spectrum in Fig. 2 (Si $3s$ and $3d$ PDOS) is approximately flat in this region with only small intensity variations. Comparing to the theoretical PDOS we see that most of the states in this energy range are associated with the Si $3d$ orbitals, with only small contributions coming from Si $3s$. The theoretical PDOS in Fig. 2 exhibit intensity variations that closely match the frequency of the variations in the ex-

perimental SXE spectra, but the relative magnitudes of these intensity variations are very different. One of the reasons for this discrepancy in the intensities between theory and experiment may be the influence of the dipole selection rules on the experimental data, which effect the Si $3s$ orbitals differently than the Si $3d$ orbitals. Thus, by normalizing the Si $L_{2,3}$ SXE spectrum to the maximum in the theoretical PDOS (located at -10 eV and corresponding to the Si $3s$ orbitals), we may underestimate the effect of the Si $3d$ orbitals in the experimental spectrum. In addition, the Mulliken decomposition we use in the calculations is not unique and it is therefore possible that some of the PDOS labeled as Si $3s$ and $3d$ could actually arise from a sum of tails from the neighboring Pt $5d$ orbitals that have either s- or d-like symmetry about the Si site. This possibility seems likely given that the peak positions in Fig. 2 match the peak positions in the Pt $5d$ PDOS shown in Fig. 4. This mixing of Pt $5d$ orbitals with Si $3s$ and $3d$ orbitals provides yet another indication that interactions with the Pt $5d$ orbitals exist over a much wider range of energies than previous models have suggested.

Both of the experimental XPS spectra in Fig. 3 ($h\nu = 80$ and 130 eV) exhibit an increase in the DOS between -8.5 and -1.0 eV. The overall intensity in this region decreases as we go to higher $h\nu$ and therefore to a first approximation we can attribute the DOS to the Pt $5d$ orbitals. The theoretical PDOS in Fig. 4 strongly support this interpretation since the Pt $5d$ orbitals are the only ones with a significant contribution to the DOS in this energy range. Previous studies have already attempted to assign each feature in this region to a different orbital configuration. The standard model described by a number of authors[49,50,53,58,59,61] is as follows: bonding and antibonding interactions between the Pt $5d$ and Si $3p$ orbitals should give rise to a structure on each side of the primary Pt $5d$ band. The feature near -6.0 eV is identified as the bonding state (labeled BS in Fig. 2) and is assumed to arise from the bonding combination of the Pt $5d$ and Si $3p$ orbitals. The corresponding antibonding state (labeled AS in Fig. 3) is located near -0.5 eV and will be discussed further in Sec. IV A 4. Finally, the primary Pt $5d$ band, or nonbonding state (labeled NS in Fig. 3), is located in between the bonding and antibonding states near -3.7 eV. This model description is based on the assumption that there is strong but incomplete mixing between the Si $3p$ and Pt $5d$ orbitals. Our experimental data and theoretical PDOS (see Fig. 3) appear to be in good accord with the previously published studies. In fact, the LDA-based calculations are consistent with both the position and the intensity of the experimental peaks, with the exception that the relative intensities of the bonding and nonbonding states are inverted. This small disagreement could arise from the fact that the σ associated with the bonding state (mixture of Si $3p$ and Pt $5d$) is small in comparison to that associated with the nonbonding state (pure Pt $5d$ state). In addition, the calculations represent only the contribution from the DOS. No attempt has been made to include dipole matrix element or final state effects and thus it can only be expected that the agreement between theory and experiment will be qualitative. Nonetheless, the overall agreement is actually quite

good given the degree of approximation. The theoretical PDOS in Fig. 4 indicate that the bonding state is a mixture of mostly Pt $5d$ with smaller contributions from Pt $6p$ as well as Si $3p$ and $3d$. Conversely, the nonbonding state is almost purely Pt $5d$ in character, with only a small contribution from Si $3p$.

Despite the qualitative and quantitative agreement with previous studies noted above, there are two small peaks in the XPS spectrum at -7.1 and -5.0 eV (labeled α and β in Fig. 3). None of the previously published work has made any mention of these features, perhaps because the experimental resolution was insufficient to allow them to be resolved or because there was no explanation for them.[61] Yarmoshenko *et al.*[67] found some intensity in these energies, but not really peaks. In Figs. 2 and 3 we can see the small intensity variations at these energies in both the theoretical PDOS and the experimental spectra. On the basis of the theoretical PDOS in Fig. 4 we see that α arises predominantly from the Pt $5d$ orbitals, with smaller contributions from Pt $6p$ as well as Si $3p$ and $3d$. Similarly, β arises predominantly from Pt $5d$ and Si $3p$, with almost no contribution from Si $3d$.

The importance of these features α and β is that their presence strongly indicates that the previously accepted idea of a relatively localized Pt $5d$ band surrounded by bonding and antibonding states may not be accurate. Instead we propose a more complex picture of the PtSi bonding in which the Pt $5d$ and Si $3p$ orbitals are strongly mixed throughout the whole VB, and where the Si $3d$ and Pt $6p$ orbitals also contribute but to a lesser extent. This idea has been mentioned recently[67] and is also supported by other x-ray emission spectroscopy and SXE measurements.

3. VB near -2.4 eV

The experimental SXE spectrum in Fig. 2 (Si $3s$ and $3d$ PDOS) exhibits a peak at -2.4 eV (labeled γ). The width of the peak is approximately 1 eV. The calculations do not reproduce the peak but there is a shoulder in the Si $3s$ and $3d$ PDOS. Since we expect a dominant Pt $5d$ band at this energy we place more emphasis on the XPS spectrum in Fig. 3 (TDOS) where there is a shoulder at -2.4 eV in both the theoretical and experimental curves. In the XPS spectrum the intensity of the shoulder increases with respect to the main peak (located at -3.7 eV and having pure Pt $5d$ character) as we increase $h\nu$, and therefore we can conclude that the shoulder is not a pure Pt $5d$ state. The theoretical curves in Fig. 3 exhibit the same shoulder located at the same energy for both the Pt and the Si PDOS. The theoretical Pt PDOS is approximately 1.6 times higher than the Si PDOS at this energy, showing that the Pt contribution is larger but that the Si contribution is still significant.

On the basis of the theoretical orbital-resolved PDOS in Fig. 4 we see that the dominant contribution to this feature comes from the Pt $5d$ orbitals, but that the Pt $6p$ and Si $3p$ orbitals also contribute in equal but lesser proportions. Rossi *et al.* reported the existence of some states associated with the Pt $5d$ orbitals at -1.8 eV.[53] These states were expected to be very localized and thus not involved in the bonding. Our results would appear to be in contradiction to the idea of a very localized state since it is well known that the Pt $6p$ orbitals are much less localized than the Pt $5d$ orbitals. Furthermore, these results provide additional support for the idea that the Pt $5d$ and $6p$ orbitals are strongly mixed with the Si $3p$ orbitals throughout the whole VB. Finally, we note that the Si $3s$ and $3d$ orbitals contribute very little to the DOS at this energy.

4. VB near -0.5 eV

Previous studies have assigned the peak located at -0.5 eV to the partially occupied antibonding state,[49,50,53,59] which is associated with the bonding state at -6.0 eV and arises from the mixture of Pt $5d$ and Si $3p$ orbitals.[53] In Fig. 2 we confirm an increase in the intensity from -0.5 eV up to E_F. A previous disagreement between theory and experiment has been reported but was related to the calculational methodology.[61] In our case the theoretical PDOS matches very well with the experimental spectrum in this energy region. As in the case of the bonding state, there are approximately equal contributions from the Si $3d$ and $3s$ orbitals. However, we again expect that the Pt $5d$ and Si $3p$ orbitals will be dominant in this energy range, and therefore greater emphasis should be placed on the XPS measurements.

In Fig. 3 there appears to be a quantitative disagreement between theory and experiment but in fact there is not. While the XPS data are given in arbitrary units, the theoretical PDOS are calculated on an absolute scale, and therefore the intensity at -0.5 eV is not close to zero. If we normalize both the theoretical and experimental peaks then the intensity close to E_F is similar (1.19 for the Pt PDOS and 1.69 for the experimental spectrum at $h\nu=80$ eV). Moreover, the experimental curve includes not only the Pt PDOS but also small contributions from the Si PDOS.

From Fig. 4 we see that only the Pt $5d$ and Si $3p$ orbitals have an appreciable PDOS in this energy range. The other orbitals contribute very little to the TDOS. This circumstance is consistent with the idea of an antibonding state. It is worthwhile reemphasizing that we have found not only qualitative, but also quantitative, agreement between theory and experiment in explaining the VB close to E_F, whereas previous studies had difficulty in this region. Finally, we mention that in the Pt PES data (not shown) the intensity at E_F is decreasing drastically, which is in accord with our calculations showing that PtSi is a poor metal, with a low TDOS at E_F.

5. CB

We have analyzed the CB (empty states) by means of XAS using the Si $L_{2,3}$ edge, which probes the unoccupied PDOS of d and s characters at the Si site. The spectrum is shown in Fig. 2 along with the theoretical PDOS. We clearly see a strong experimental peak at 1 eV above E_F that is reproduced with less intensity by the calculations. This peak has primarily Si $3d$ character but also a small Si $3s$ contribution. However, it is unlikely that the Si $3s$ orbitals would contribute in this energy range and therefore it is more probable that this s-like PDOS arises from either the Si $4s$ orbitals or an s-like combination of Pt $5d$ tails from neighboring
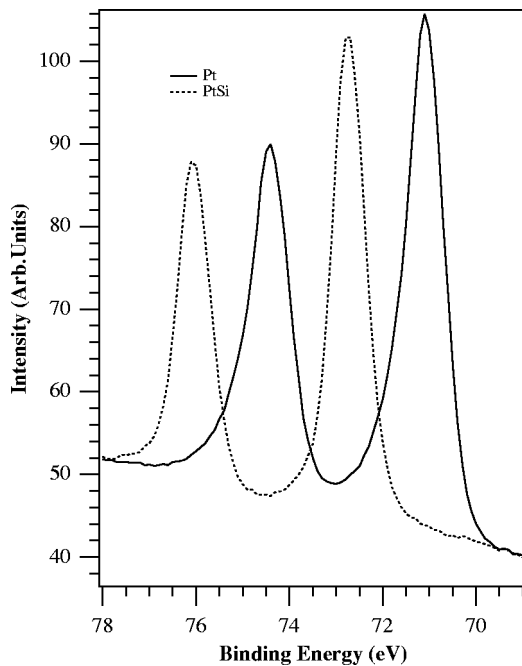
FIG. 5. Pt $4f$ CL-PES data obtained at $h\nu = 130$ eV for both pure Pt (solid line) and a thick film (<100 Å) of PtSi (dotted line) that was prepared *in situ* on Si(100) by evaporation of Pt and annealing. The shift between the two sets of spin-orbit-split peaks is 1.7 eV, in good agreement with previously published data (Ref. 51).

sites. Overall the theoretical PDOS agrees reasonable well with the experimental spectrum and with the previously published data of Naftel *et al.*[62]

B. Si $2p$ and Pt $4f$ core level spectroscopy

Measurements of the VB electronic structure only provide information about the outermost valence orbitals but they yield no information about the charge transfer between atoms. Study of the core levels is therefore a means of obtaining additional knowledge about the electronic structure of a material. However, the analysis of core level data can be complex because any spectrum must be compared to a reference sample. In this section we report an experimental study of the Pt $4f$ and Si $2p$ core levels for a thick PtSi film prepared *in situ*, and we compare our results with previously published data.

In Fig. 5 we show the Pt $4f$ core level for pure Pt as well as PtSi, both obtained at $h\nu = 130$ eV. At this energy the EED and σ are both close to their respective minima and therefore there is a trade off between high surface sensitivity (low EED) and low Pt $4f$ cross section σ. From the data in Fig. 5 we see a shift to higher binding energy ($\Delta E = 1.7$ eV) in PtSi relative to pure Pt. This shift has been reported by different authors,[50,54] and our measurements agree very well with these previously published data. Given these results we can conclude that our data correspond to a pure PtSi sample and not a mixture of PtSi and Pt$_2$Si. This conclusion is based on the fact that the core level shift associated with Pt$_2$Si is 1.2 eV,[50] as well as the absence of any other core level component or shoulder in our data.

A bigger core level shift between Pt and PtSi as compared to the corresponding shift for Pt$_2$Si is consistent with the chemical bonding in these two materials. Klepeis *et al.*[65] have shown that there are a relatively small number of strong Pt-Si covalent bonds in PtSi, whereas Pt$_2$Si contains a much larger density of much weaker covalent bonds, in addition to two-dimensional Pt-Pt metallic bonding. The chemical bonding environment of the Pt atoms in Pt$_2$Si is therefore more similar to that of pure Pt than is the case for the Pt atoms in PtSi. Since the respective core level shifts in the silicides relative to pure Pt reflect this local bonding environment, it is not surprising that the shift for Pt$_2$Si is smaller than that for PtSi.

Both of the core level peaks in Fig. 5 exhibit an asymmetric line shape, which is characteristic of metals. The photoemission intensity from a core level corresponds to a Voigt line shape where the Lorentzian linewidth is determined by the lifetime of the core hole. In metals this intensity is modified by the creation of electron-hole pairs that result in an asymmetric Doniach-Sunjic line shape.[88] The observed asymmetry in the Pt $4f$ core level for PtSi provides additional confirmation of the purity of our sample. We also note that the linewidth of the pure Pt core level peak is larger than that for PtSi. This effect is due to the enhanced screening of the photoemitted electron in pure Pt, and has been reported previously.[50] Thus we are able to conclude that our PtSi sample was pure with no contaminants. In addition, the metallic nature of the film is confirmed by the core level line shape.

We can obtain qualitative information about the charge transfer between the Pt and Si atoms by integrating the respective theoretical PDOS for the two atoms. This analysis indicates a sizable transfer of charge from the Si orbitals to the Pt orbitals. This sign for the charge transfer would appear on the surface to disagree with the shift of the Pt $4f$ core level to higher binding energy. However, the core level shift results from the overall redistribution of electronic charge, which in the case of PtSi corresponds to the formation of strong Pt-Si covalent bonds as opposed to the Pt-Pt metallic bonding in pure Pt. Such a complex redistribution of the electronic charge can in principle produce a core level shift of either sign. Additional analysis of the individual orbital contributions to the theoretical PDOS for both pure Pt and PtSi indicates that relative to the neutral Pt atoms in pure Pt there is a loss of Pt $5d$ charge in PtSi, but that this loss is more than compensated for by a significant increase in Pt $6p$ charge. There is also a small increase in the Pt $5f$ contribution while Pt $6s$ is essentially unchanged.

The Si $2p$ core level measurements for PtSi in Fig. 6 exhibit a much more complex structure than the Pt $4f$ core level measurements. For reference purposes we also measured the Si $2p$ core level corresponding to the clean Si(100)(2×1) surface. The atomic and electronic structure of this clean surface is completely understood, and a well resolved CL-PES peak can be fit with five Voigt functions[89] corresponding to five different components. Only one of these components corresponds to bulk Si (labeled B in Fig. 6) while the others correspond to surface and near-surface atoms. We also note that in our clean Si(100)(2×1) spec-
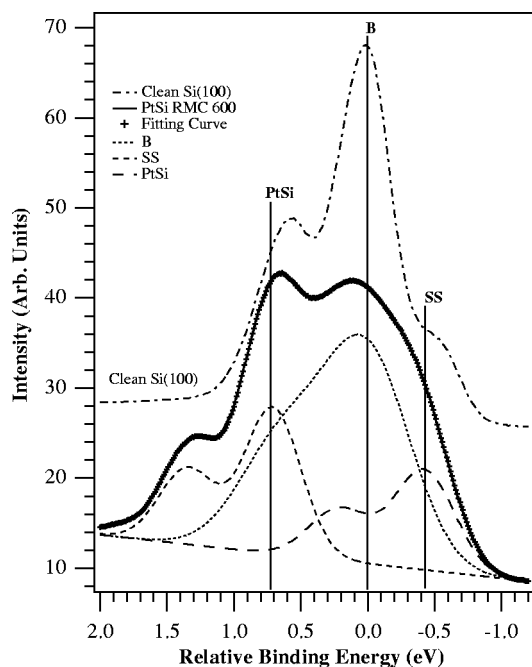
FIG. 6. Si $2p$ CL-PES for clean Si(100)(2×1) (top) and PtSi/Si(100) (bottom). We also show the curve fit for the PtSi case (crosses). Using only PtSi, bulk (B), and surface state (SS—tentative assignment) components we are able to achieve a close fit.

trum (Fig. 6) a surface state clearly appears approximately 0.5 eV toward a lower binding energy from the bulk peak (labeled SS), providing a strong indication of a clean surface. The curve corresponding to the clean Si(100)(2×1) surface was fit and yielded similar parameters to those reported by Landemark *et al.*[89]

The fit for the Si $2p$ CL-PES of PtSi is also shown in Fig. 6, and it has three components. We assign the high binding energy peak to PtSi and the middle peak to bulk Si. The origin of the low binding energy peak is somewhat uncertain, but we note that it occurs at approximately the same energy as the surface state of the clean surface and so we tentatively make this assignment. The Si $2p$ core level shift for PtSi relative to clean Si(100)(2×1) has been measured previously and found to be 1.0 eV toward higher binding energy.[52] Our fit yields a core level shift of 0.74 eV, providing support for our assignment of the two higher binding energy peaks. The apparent presence of a bulk Si core level component, and possibly a clean surface state as well, would seem to suggest that the Si(100)/PtSi interface is not well formed. According to the kinetic model for the formation of PtSi on a Si substrate (described in Sec. III and illustrated schematically in Fig. 1), the first step that must take place is the deposited Pt atoms must migrate into the Si substrate and form Pt_2Si. The second step is for substrate Si atoms to diffuse back into the Pt_2Si to form PtSi. If the Si/PtSi interface were "perfect" then we would not expect any trace of bulk Si to appear in the core level spectrum. The presence of these components can be explained if the annealing time was too long or the annealing temperature too high. It has been reported[86] that increasing the annealing time or temperature beyond the minimum that are needed can lead to diffusion of excess Si into the PtSi film. This excess Si diffusion could result in a film composed of PtSi regions and bulklike Si regions. The minimum annealing time and temperature needed to form PtSi are very sensitive to the defects, impurities, and inhomogeneity of the annealing, and therefore it is very possible that we overannealed the sample just enough to create fragments of bulk-like Si at or close to the film surface. Excess Si migration has been discussed as part of a larger study of the effects of cleanliness on the formation of PtSi on a Si substrate.[86]

Interestingly, we find a core level double shift, meaning that the shift for the Si $2p$ core level is in the same direction as that for the Pt $4f$ core level, compared to the Si and Pt references, respectively. We have also carried out first principles calculations that confirm the presence of a core level double shift. As we indicated above, the complex redistribution of electronic charge into strong covalent bonds can result in core level shifts of either sign. An analysis of our theoretical PDOS has indicated that this double shift can also be interpreted in terms of a charge compensation mechanism in which the Pt in PtSi loses $5d$ electrons but that this loss is overcompensated by the gain of $6p$ electrons so that the overall flow of electronic charge is from Si to Pt. Naftel *et al.*[62] have previously found a similar double shift measured with Si K-edge and Pt $M_{2,3}$-edge x-ray absorption near-edge structure (XANES) (in TEY). On the basis of these experiments and additional PES data they also suggested a charge compensation mechanism with Pt losing a $5d$ and gaining a non-d electron. The idea of a complex rearrangement of charge is consistent with our conclusion that the previously accepted standard model of bonding in the silicides is not correct, at least for PtSi. Rather than a simple transfer of charge between the two atom types in the unit cell, we have instead found multiple reasons to infer a much more complex reconfiguration of the charge into covalent bonds. The presence of a core level double shift is just one more piece of evidence supporting the idea that the Pt $5d$ orbitals are not highly localized but instead are strongly mixed with the Si orbitals.[90]

C. Electronic charge density and chemical bonds

Our study of the experimental and theoretical PDOS has led us to the conclusion that the Pt $5d$ orbitals are not highly localized as has been assumed in all previous experimental studies of PtSi. Rather we have found evidence that the influence of the d orbitals extends throughout the whole VB and that the nature of the chemical bonds is more complex than the earlier studies assumed. This conclusion is very strongly supported by a recent study of Klepeis *et al.*[65] in which an analysis of the electronic charge density revealed evidence of a small number of strong Pt-Si covalent bonds. They also analyzed the elastic constants of PtSi, which enabled an estimate of the strength of these bonds. The covalent bonds in PtSi were found to be nearly as strong as the Si-Si bonds in pure Si. However, the bond angles in PtSi are significantly distorted away from the tetrahedral angles of pure Si, which resulted in the striking appearance of three-center Pt-Si-Pt bonds, in addition to more usual two-center Pt-Si bonds.
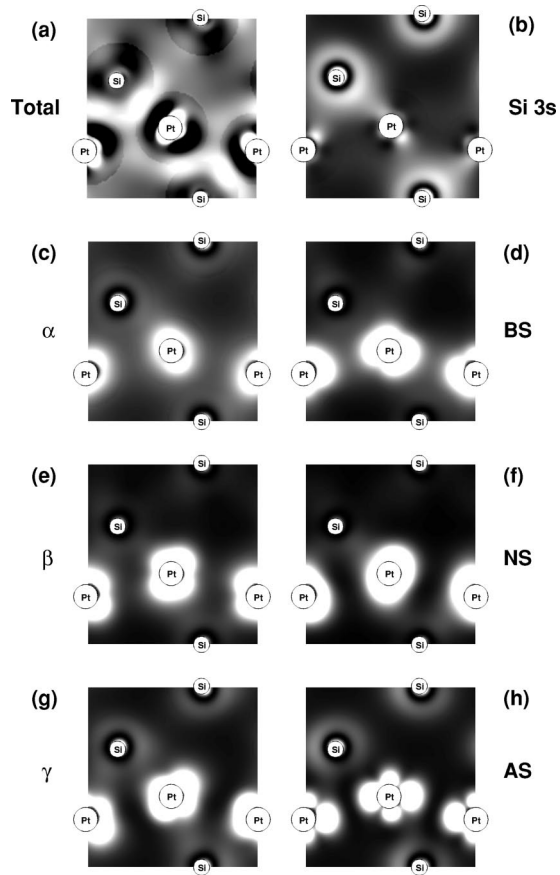
FIG. 7. Energy-resolved electronic charge density corresponding to the seven PDOS features (energy windows) discussed in connection with Figs. 2–4. The total electronic charge density is given in panel (a) and is equal to the sum of the densities in the remaining seven panels, which are labeled according to their respective PDOS features. The plane of the plots corresponds to a **b**-axis slice through the unit cell. In all cases black corresponds to the lowest electron density and white to the highest density. The highest density for each panel has been cut off in order to focus on the density in the interesting bonding regions in between the atoms. These cutoff values have been chosen to scale with the total number of valence electrons in each of the respective energy windows.

In order to connect the bonding information deduced from the real-space electronic charge density with the **k**-space PDOS information discussed in the present study, we have decomposed the total charge density into energy-resolved contributions corresponding to the various features in the VB PDOS discussed in Sec. IV A above. The sum of all these energy-resolved contributions yields the total charge density, but by looking at the energy dependence we can gain additional insight into the nature of the electronic states at different energies. In Fig. 7 we show the energy-resolved charge densities corresponding to each of the PDOS features discussed above. In all cases black corresponds to the lowest density and white to the highest density. The plane of the plots corresponds to a **b**-axis slice through the unit cell containing two Pt atoms and two Si atoms (as well as one Pt and one Si periodic image).

Figure 7(a) shows the total valence charge density. In Ref. 65 the free-atom charge density was subtracted from the total

valence charge density in order to emphasize the formation of bonds. In the present context we have plotted the valence density directly in order to facilitate the comparison with the energy-resolved densities where it is not sensible to subtract out a free-atom contribution. One consequence of plotting the full valence density is that there is a rather large pile-up of charge close the atoms, especially the Pt atoms. This large pile-up arises from the fact that we are using an all-electron method and the wave functions have large oscillations near the atom cores. These oscillations are not of direct interest but rather we wish to focus on the density in between the atoms where the chemical bonding is active. For this reason each of the plots is cut off at a particular magnitude of the density in order to emphasize the bonding regions. A difficulty then arises in choosing an appropriate cutoff for each of the plots. It is not sensible to use the same cutoff in each case because the total integrated charge corresponding to the individual energy windows is different for all eight plots. For example, the total valence charge corresponding to Fig. 7(a) is 56 electrons, while the integrated charge in the case of Fig. 7(b) is only eight electrons. We have therefore chosen to scale the cutoff for each plot by the total amount of charge in each of the respective energy windows.

The three-center Pt-Si-Pt bonds discussed in Ref. 65 are also visible in Fig. 7(a). One of these bonds involves the leftmost Si atom in the plot and its two near-neighbor Pt atoms. The remaining seven panels in Fig. 7 correspond to the seven PDOS features shown in Figs. 2–4 and are labeled accordingly. Once again, the sum of these seven energy-resolved contributions adds up to give the total valence charge density in the first panel. The energy-resolved charge density in Fig. 7(b) corresponds to the Si 3s-dominated PDOS feature at -10 eV. As in the analysis of the PDOS we can clearly see that the Si 3s orbitals are dominant but there is also strong evidence of a charge pile-up between the Pt and Si atoms as well as d- or possibly p-like contributions arising from the Pt atoms. This result, in direct contradiction to previous models, provides a strong indication that the Si 3s orbitals participate in the Pt-Si bonds and that the influence of the Pt orbitals extends all the way to the bottom of the valence band. As another example, Fig. 7(f) shows the energy-resolved charge density corresponding to the PDOS feature labeled NS in Fig. 3, which has been associated with a nonbonding combination of Pt 5d orbitals in earlier studies. Although the contribution from the Pt 5d orbitals is certainly dominant, consistent with the theoretical PDOS in Fig. 4, we nonetheless see a pile-up of charge between the Pt and Si atoms. This result again demonstrates that the Pt d orbitals are not strongly localized but rather that they are active participants in strong Pt-Si covalent bonds. In general, each of the plots in Fig. 7 show, to a greater or lesser extent, that the Pt-Si bonding in PtSi is extended essentially throughout the entire VB.

V. SUMMARY AND CONCLUSIONS

We have carried out a combined experimental and theoretical characterization of the PtSi electronic structure using SR-PES, SXE, XAS, and first principles electronic structure

calculations. SXE and XAS measurements of the Si $L_{2,3}$ edge have allowed us to probe the Si $3s$ and $3d$ PDOS in the VB and CB. Additional SR-PES measurements of the VB were obtained at $h\nu = 80$ and 130 eV. By comparing the spectra at these two photon energies we were able to probe the contribution of the Pt $5d$ orbitals by means of the Cooper minimum effect. In each case first principles calculations of the PDOS for the Pt $6p$ and $5d$ as well as the Si $3s$, $3p$, and $3d$ orbitals have enabled us to provide a detailed interpretation of the experimental spectra. We have also performed Pt $4f$ and Si $2p$ CL-PES measurements that have provided information about the charge transfer between the Pt and Si and thus give additional insight into the nature of the chemical bonding in PtSi. Finally, first principles calculations of the energy-resolved electronic charge density have allowed us to connect the **k**-space spectroscopic information with the real-space chemical bonds.

To date the generally accepted model for the chemical bonding in transition-metal silicides, including PtSi, is that bonding and antibonding interactions between the transition-metal d and Si $3p$ orbitals should give rise to a structure on each side of the primary d band. This model description is based on the assumption that there is strong but incomplete mixing between the Si $3p$ and transition-metal d orbitals. Our XPS measurements exhibit peaks that have previously been identified as bonding, nonbonding, and antibonding states at -6.0, -3.7, and -0.5 eV, respectively. The bonding and antibonding states are primarily mixtures of the Pt $5d$ and Si $3p$ orbitals while the nonbonding state is almost purely Pt $5d$. Our experimental data and theoretical PDOS are in accord with previous studies, although the calculations also indicate small contributions to the bonding state from the Pt $6p$ and Si $3d$ orbitals. In contrast to earlier studies, we have found good agreement between our SXE and XPS measurements and the theoretical PDOS for the nonbonding state near E_F. We also note that the theoretical PDOS agrees reasonably well with the experimental XAS spectrum of the CB states near E_F.

Despite the qualitative and quantitative agreement with previous studies noted above, a closer examination of the experimental spectra reveals features that do not fit into the generally accepted chemical bonding model. Two examples are the peaks in the XPS spectrum at -7.1 and -5.0 eV that we have labeled α and β. The SXE spectrum also shows small intensity variations at these same energies. These peaks have not been discussed in any of the previous studies of PtSi, to our knowledge. We find that α arises predominantly from the Pt $5d$ orbitals, with smaller contributions from Pt $6p$ as well as Si $3p$ and $3d$, while β arises predominantly from Pt $5d$ and Si $3p$, with almost no contribution from Si $3d$. In addition, the experimental SXE spectrum exhibits a peak at -2.4 eV that we have labeled γ. The XPS spectrum and the theoretical PDOS have a shoulder at this same energy. This feature has been previously mentioned in passing as arising from very localized orbitals and thus was not expected to be involved in the bonding. However, we find that although the dominant contribution comes from the Pt $5d$ orbitals there are, nonetheless, significant contributions from the Pt $6p$ and Si $3p$ orbitals. These latter orbitals are not

expected to be strongly localized. Finally, the prominent peak in the SXE spectrum near -10 eV is well documented and has been associated purely with the Si $3s$ orbitals. It is universally assumed that these orbitals are also not involved in the bonding but we have found strong experimental and theoretical evidence that at least some mixing between the Si $3s$ and Pt $5d$ or $6p$ orbitals occurs in this energy range. All three of these findings strongly indicate that the previously accepted chemical bonding model is not accurate. Rather we propose a more complex picture of the PtSi bonding in which the Pt $5d$ and Si $3p$ orbitals are strongly mixed throughout the whole VB, and where the Si $3d$ and Pt $6p$ orbitals also contribute but to a lesser extent.

Additional information about the nature of the chemical bonding is provided by the Pt $4f$ and Si $2p$ CL-PES measurements. We find a 1.7 eV shift of the Pt $4f$ core level to higher binding energy in PtSi relative to pure Pt, which agrees very well with previously published data. The fact that we find only one Pt $4f$ core level component allows us to conclude that our data correspond to a pure PtSi sample and not a mixture of PtSi and Pt$_2$Si. The observed asymmetric Doniach-Sunjic line shape for the Pt $4f$ core level confirms the metallic nature of the PtSi thin film. In the case of the Si $2p$ core level we are able to achieve a good fit to our PES data for PtSi with three components corresponding to PtSi, bulk Si, and a tentative surface state. Our Si $2p$ core level shift for PtSi relative to clean Si(100)(2×1) is 0.74 eV to higher binding energy, which is somewhat smaller than the previously measured value. First principles calculations confirm the presence of a core level double shift in which both the Pt $4f$ and Si $2p$ core levels shift to higher binding energy. The apparent presence of a bulk Si core level component suggests that the Si(100)/PtSi interface is not well formed. It is possible that we overannealed the sample during the formation of the PtSi film such that excess Si migrated into the film and created fragments of bulk-like Si at or close to the surface.

The fact that we find a core level double shift means that there is not a simple transfer of charge between the two atom types in the unit cell. We have analyzed the theoretical PDOS and find evidence of a sizable net transfer of charge from the Si orbitals to the Pt orbitals. However, the core level shifts result from the overall redistribution of electronic charge, which in the case of PtSi corresponds to the formation of strong three-center Pt-Si-Pt and two-center Pt-Si covalent bonds. This complex redistribution of electronic charge in PtSi can in principle result in core level shifts of either sign. A further analysis of our theoretical PDOS has indicated that this double shift can also be interpreted in terms of a charge compensation mechanism in which the Pt in PtSi loses $5d$ electrons, but that this loss is overcompensated for by the gain of $6p$ electrons so that the overall flow of electronic charge is from Si to Pt. The idea of a complex rearrangement of charge is consistent with our proposal that the previously accepted chemical bonding model for the transition-metal silicides is not correct, at least for PtSi. Once again, we infer that the Pt $5d$ orbitals are not highly localized but instead are strongly mixed with the Si orbitals.

Our first principles calculations of the energy-resolved charge density have provided further evidence for the more complex and distributed nature of the chemical bonding in PtSi. These calculations revealed that contributions to the strong three-center Pt-Si-Pt and two-center Pt-Si covalent bonds in PtSi are extended throughout the entire VB. In conclusion, our combined experimental and theoretical study of the electronic structure of PtSi has led us to propose that the Pt $5d$ orbitals are not highly localized as has been assumed in all previous experimental studies of PtSi. Rather we find that the influence of the $5d$ orbitals extends throughout the whole VB, and that the nature of the chemical bonds is more complex than the earlier studies assumed.

[1] M. P. Lepselter and J. M. Andrews, in *Ohmic Contacts to Semiconductors*, edited by B. Schwartz, (The Electrochemical Society, New York, NY, 1969).

[2] E. H. Rhoderick and R. H. Williams, *Metal-Semiconductor Contacts* (Oxford University Press, Oxford, 1988).

[3] *Proceedings of 1991 European Workshop on Refractory Metals and Silicides, Saltsjobaden, Sweden, March 1991*, Appl. Surf. Sci. **53**, (1991), and references therein.

[4] S. R. Murarka, *Metalization: Theory and Practice for VLSI Applications* (Butterworth-Heinemann, Boston, 1993).

[5] A. K. Sinha, R. B. Marcus, T. T. Sheng, and S. E. Haszko, J. Appl. Phys. **43**, 3637 (1972).

[6] S. R. Murarka, *Silicides for VLSI Applications* (Academic, New York, 1983).

[7] P. W. Pellegrini, C. E. Ludington, and M. M. Weeks, J. Appl. Phys. **67**, 1417 (1990).

[8] A. Tanabe, K. Konuma, N. Teranishi, S. Tohyama, and K. Masubuchi, J. Appl. Phys. **69**, 850 (1991).

[9] M. Wittmer, Phys. Rev. B **43**, 4385 (1991).

[10] A. Czernik, H. Palm, W. Cabanski, M. Schulz, and U. Suckow, Appl. Phys. A: Solids Surf. **55**, 180 (1992).

[11] L. P. Wang, J. R. Yang, and J. Hwang, J. Appl. Phys. **74**, 6251 (1993).

[12] V. W. L. Chin, J. W. V. Storey, and M. A. Green, Solid-State Electron. **39**, 277 (1996).

[13] K. Solt, H. Melchior, U. Kroth, P. Kuschnerus, V. Persch, H. Rabus, M. Richter, and G. Ulm, Appl. Phys. Lett. **69**, 3662 (1996).

[14] M. Razeghi and A. Rogalski, J. Appl. Phys. **79**, 7433 (1996), and references therein.

[15] C.-A. Chang, J. Appl. Phys. **58**, 3258 (1985).

[16] C.-A. Chang and A. Segmüller, J. Appl. Phys. **61**, 201 (1987).

[17] D. Drouin, J. Beauvais, R. Lemire, E. Lavallée, R. Gauvin, and M. Caron, Appl. Phys. Lett. **70**, 3020 (1997).

[18] K. L. Saenger, A. Grill, and C. Cabral, Jr., J. Mater. Res. **13**, 462 (1998).

[19] *Advanced interconnects and contacts*, edited by D. C. Edelstein *et al.* (Materials Research Society, Warrendale, PA, 1999), and references therein.

[20] C. Blair, E. Demirlioglu, E. Yoon, and J. Pierce, *Silicides, Germanides and their Interfaces*, edited by R. W. Fathauer, L. Schowalter, S. Mantl, and K. N. Tu, MRS Symposia Proceedings No. 320 (Materials Research Society, Pittsburgh, 1994).

[21] D.-X. Xu, S. R. Das, L. Erickson, and A. Naem, *Materials Reliability in Microelectronics V*, edited by A. S. Oates, W. F. Filter, R. Rosenberg, A. L. Greer, and K. Gadepally, MRS Symposia Proceedings No. 391 (Materials Research Society, Pittsburgh, 1995), p. 223.

[22] D.-X. Xu, J. P. McCaffrey, S. R. Das, G. C. Aers, and L. E. Erickson, Appl. Phys. Lett. **68**, 3588 (1996).

[23] C. Canali, F. Catellani, M. Prudenziati, W. H. Wadlin, and C. A. Evans, Jr., Appl. Phys. Lett. **31**, 43 (1977).

[24] C. Canali, F. Catellani, G. Ottaviani, and M. Prudenziati, Appl. Phys. Lett. **33**, 187 (1978).

[25] A. Prabhakar, T. C. McGill, and M.-A. Nicolet, Appl. Phys. Lett. **43**, 1118 (1983).

[26] D. Wang, A. J. Freeman, and H. Krakauer, Phys. Rev. B **29**, 1665 (1984).

[27] R. Matz, R. J. Purtell, Y. Yokota, G. W. Rubloff, and P. S. Ho, J. Vac. Sci. Technol. A **2**, 253 (1984).

[28] R. Pretorius, M. A. E. Wandt, J. E. McLeod, A. P. Botha, and C. M. Comrie, J. Electrochem. Soc. **136**, 839 (1989).

[29] J. E. McLeod, M. A. E. Wandt, R. Pretorius, and C. M. Comrie, J. Appl. Phys. **72**, 2232 (1992).

[30] T. Stark, H. Grünleitner, M. Hundhausen, and L. Ley, Thin Solid Films **358**, 73 (2000).

[31] J. M. Poate and T. C. Tisone, Appl. Phys. Lett. **24**, 391 (1974).

[32] M. Wittmer, J. Appl. Phys. **54**, 5081 (1983).

[33] S. Mantovani, F. Nava, C. Nobili, M. Conti, and G. Pignatel, Appl. Phys. Lett. **44**, 328 (1984).

[34] S. M. Zhou, M. Hundhausen, T. Stark, L. Y. Chen, and L. Ley, J. Vac. Sci. Technol. A **17**, 144 (1999).

[35] J. B. Bindell, J. W. Colby, D. R. Wonsidler, J. M. Poate, D. K. Conley, and T. C. Tisone, Thin Solid Films **37**, 441 (1976).

[36] P. Joubert, P. Auvray, A. Guivarc'h, and G. Pelous, Appl. Phys. Lett. **31**, 753 (1977).

[37] C. A. Crider and J. M. Poate, Appl. Phys. Lett. **36**, 417 (1980).

[38] C. Harder, L. Hammer, and K. Muller, Phys. Status Solidi A **146**, 385 (1994).

[39] R. Schmiedl, V. Demuth, P. Lahnor, H. Godehardt, Y. Bodschwinna, C. Harder, L. Hammer, H. P. Strunk, M. Schulz, and K. Heinz, Appl. Phys. A: Mater. Sci. Process. **62**, 223 (1996).

[40] K. L. Kavanagh, M. C. Reuter, and R. M. Tromp, J. Cryst. Growth **173**, 393 (1997).

[41] M. Wittmer, W. Lüthy, and M. von Allmen, J. Appl. Phys. **51**, 5386 (1980).

[42] H. B. Ghozlene, P. Beaufrère, and A. Authier, J. Appl. Phys. **49**, 3998 (1978).

[43] T. T. Tsong, S. C. Wang, F. H. Liu, H. Cheng, and M. Ahmad, J. Vac. Sci. Technol. B **1**, 915 (1983).

[44] R. J. Nemanich, C. M. Doland, and F. A. Ponce, J. Vac. Sci. Technol. B **5**, 1039 (1987).

[45] R. W. Fathauer, Q. F. Xiao, S. Hashimoto, and C. W. Nieh, Appl. Phys. Lett. **57**, 686 (1990).

[46] K. Konuma and H. Utsumi, J. Appl. Phys. **76**, 2181 (1994).

[47] B. A. Morgan, K. M. Ring, K. L. Kavanagh, A. A. Talin, R. S. Williams, T. Yasuda, T. Yasui, and Y. Segawa, J. Vac. Sci. Technol. B **14**, 1238 (1996).

[48] C. Kumpf, R. Nicula, and E. Burkel, J. Appl. Crystallogr. **30**, 1016 (1997).

[49] G. Rossi, I. Abbati, L. Braicovich, I. Lindau, and W. E. Spicer, Solid State Commun. **39**, 195 (1981).

[50] P. J. Grunthaner, F. J. Grunthaner, and A. Madhukar, J. Vac. Sci. Technol. **20**, 680 (1982).

[51] P. J. Grunthaner and F. J. Grunthaner, J. Vac. Sci. Technol. **21**, 637 (1982).

[52] G. Rossi, I. Abbati, L. Braicovich, I. Lindau, and W. E. Spicer, Phys. Rev. B **25**, 3627 (1982).

[53] G. Rossi, Surf. Sci. Rep. **7**, 1 (1987).

[54] D.-X. Dai and I. Davoli, Vacuum **44**, 1189 (1993).

[55] P. Morgen, B. Jørgensen, and J. Gordon, Phys. Scr. **T54**, 278 (1994).

[56] P. Morgen, M. Szymonski, J. Onsgaard, B. Jørgensen, and G. Rossi, Surf. Sci. **197**, 347 (1988).

[57] L. Braicovich, I. Abbati, J. N. Miller, I. Lindau, S. Schwarz, P. R. Skeath, C. Y. Su, and W. E. Spicer, J. Vac. Sci. Technol. **17**, 1005 (1980).

[58] I. Abbati, L. Braicovich, B. De Michelis, O. Bisi, and R. Rovetta, Solid State Commun. **37**, 119 (1981).

[59] G. W. Rubloff, Phys. Rev. B **25**, 4307 (1982).

[60] R. Purtell, G. Hollinger, G. W. Rubloff, and P. S. Ho, J. Vac. Sci. Technol. A **1**, 566 (1983).

[61] S. Yamauchi, S. Kawamoto, M. Hirai, M. Kusaka, M. Iwami, H. Nakamura, H. Ohshima, and T. Hattori, Phys. Rev. B **50**, 11 564 (1994).

[62] S. J. Naftel, I. Coulthard, T. K. Sham, D.-X. Xu, L. Erickson, and S. R. Das, Thin Solid Films **309**, 580 (1997).

[63] S. J. Naftel, A. Bzowski, T. K. Sham, D.-X. Xu, and S. R. Das, J. Phys. IV **7**, C2-1131 (1997).

[64] O. Beckstein, J. E. Klepeis, G. L. W. Hart, and O. Pankratov, Phys. Rev. B **63**, 134112 (2001).

[65] J. E. Klepeis, O. Beckstein, O. Pankratov, and G. L. W. Hart, Phys. Rev. B **64**, 155110 (2001).

[66] O. Bisi and C. Calandra, J. Phys. C **14**, 5479 (1981).

[67] Y. M. Yarmoshenko, S. N. Shamin, L. V. Elokhina, V. E. Dolgih, E. Z. Kurmaev, S. Bartkowski, M. Neumann, D. L. Ederer, K. Göransson, B. Noläng, and I. Engström, J. Phys.: Condens. Matter **9**, 9403 (1997).

[68] N. Franco, J. E. Klepeis, C. Bostedt, T. Van Buuren, C. Heske, O. Pankratov, and L. J. Terminello, J. Electron Spectrosc. Relat. Phenom. **114-116**, 1191 (2001).

[69] J. Stöhr, *NEXAFS Spectroscopy* (Springer-Verlag, Berlin, 1992).

[70] T. A. Callcott, *Experimental Methods in the Physical Sciences* (Academic, New York, 1998), Vol. 32, p. 279.

[71] S. Húfner, *Photoelectron Spectroscopy* (Springer-Verlag, Berlin 1995).

[72] P. J. W. Weijs, M. T. Czyżyk, J. F. van Acker, W. Speier, J. B. Goedkoop, H. van Leuken, H. J. M. Hendrix, R. A. de Groot, G. van der Laan, K. H. J. Buschow, G. Wiech, and J. C. Fuggle, Phys. Rev. B **41**, 11 899 (1990).

[73] By taking data from a polycrystalline sample and with an angle integrated spectrometer the matrix element effects due to the polarization of the light are removed, meaning that the VB spectra can be interpreted in terms of the TDOS.

[74] There are only two factors if we neglect the polarization of the light, restrict ourselves to polycrystalline samples, and use an angle integrated spectrometer.

[75] J. W. Cooper, Phys. Rev. **128**, 681 (1962).

[76] D. E. Eastman, J. J. Donelon, N. C. Hien, and F. J. Himpsel, Nucl. Instrum. Methods **172**, 327 (1980).

[77] J. J. Jia, T. Callcott, J. Yurkas, A. W. Ellis, F. J. Himpsel, M. G. Samant, J. Stöhr, D. L. Ederer, J. A. Carlisle, E. A. Hudson, L. J. Terminello, D. K. Shuh, and R. C. Perera, Rev. Sci. Instrum. **66**, 1394 (1995).

[78] M. Methfessel, Phys. Rev. B **38**, 1537 (1988).

[79] M. Methfessel, C. O. Rodriguez, and O. K. Andersen, Phys. Rev. B **40**, 2009 (1989).

[80] D. M. Ceperley and B. J. Alder, Phys. Rev. Lett. **45**, 566 (1980).

[81] S. H. Vosko, L. Wilk, and M. Nusair, Can. J. Phys. **58**, 1200 (1980).

[82] P. E. Blöchl, O. Jepsen, and O. K. Andersen, Phys. Rev. B **49**, 16 223 (1994).

[83] E. J. Graeber, R. J. Baughman, and B. Morosin, Acta Crystallogr., Sect. B: Struct. Crystallogr. Cryst. Chem. **29**, 1991 (1973).

[84] R. S. Mulliken, J. Chem. Phys. **23**, 1833 (1955).

[85] A. K. McMahan, J. E. Klepeis, M. van Schilfgaarde, and M. Methfessel, Phys. Rev. B **50**, 10 742 (1994).

[86] N. Franco, C. Bostedt, T. Van Buuren, and L. J. Terminello (unpublished).

[87] For reference purposes we measured SXE and XAS spectra from a p-type Si sample doped with a density of $4 \times 10^{13}/\mathrm{cm}^3$ acceptors. E_F for this sample is 0.3 eV above the VB maximum. Using the elastic peak (SXE) and adjusting the Si $2p$ threshold to be at 99.5 eV (XAS) we can calibrate the energy levels of the remaining spectra (we took the Si band gap to be 1.1 eV).

[88] J. Joyce, M. del Giudice, and J. H. Weaver, J. Electron Spectrosc. Relat. Phenom. **49**, 31 (1989).

[89] E. Landemark, C. J. Karlsson, Y.-C. Chao, and R. I. G. Uhrberg, Phys. Rev. Lett. **69**, 1588 (1992).

[90] We note that the formation of covalent bonds does correspond to a certain degree of spatial localization but this localization is still much less than has been previously assumed. In earlier works the Pt $5d$ orbitals were assumed to be so localized that there was very little interaction with the Si orbitals. Conversely, the formation of covalent bonds implies a strong interaction.